



ELSEVIER

Contents lists available at ScienceDirect

Scientific African

journal homepage: [www.elsevier.com/locate/sciaf](http://www.elsevier.com/locate/sciaf)

## Mineralogical and petrographic characterisation of flake graphite in the graphite mica schist rocks from the Nubian Desert, Sudan

Dalal Desouqi<sup>a,\*</sup>, Mohamad Amran Mohd Salleh<sup>a</sup>, Muhammad Hatta Roselee<sup>b</sup>,  
Aisyah M Yahya<sup>a</sup>, Bushra Abdo Alsalam<sup>c</sup>, Suraya Abdul Rashid<sup>a</sup>

<sup>a</sup> Department of Chemical and Environmental Engineering, Faculty of Engineering, Universiti Putra Malaysia, 43400 UPM Serdang, Selangor Darul Ehsan, Malaysia

<sup>b</sup> Department Of Geology, Faculty of Science, Universiti Malaya, 50603 Kuala Lumpur, Malaysia

<sup>c</sup> Department of Geology, Faculty of Petroleum & Minerals, Al Neelain University, El Gamhuriya Avenue, Khartoum, Sudan

### ARTICLE INFO

Editor: DR B Gyampoh

#### Keywords:

Mineralogy  
Petrography  
Graphite  
Flake graphite  
Graphite schist  
Nubian desert  
Sudan

### ABSTRACT

The Nubian Desert in Sudan, spanning from the Nile River in Wadi Halfa to the eastern Red Sea region, hosts graphite-bearing rocks that can potentially meet the increasing demand for natural graphite, a critical mineral in green energy technologies. This study is the first to investigate the detailed mineralogical and petrographic characteristics of graphite-bearing rocks from this region using petrography, scanning electron microscopy (SEM), energy-dispersive X-ray spectrometry (EDX), X-ray diffraction (XRD), and thermogravimetric analysis (TGA). The Nubian Desert flake graphite is of high-grade and hosted in metamorphic graphite schist that has been subjected to an increasing regional environment of amphibolite-to-greenschist facies. The schist is of high-grade and fine-grained, with a clear foliation texture composed of graphite (10 %), quartz (35 %), mica (biotite+muscovite) (50 %), and albite (5 %). Fine graphite flakes, ranging from 50 to 150  $\mu\text{m}$  in length with an average width of 46  $\mu\text{m}$ , are disseminated along the schist foliation texture. The quantitative elemental contents are C (10 %),  $\text{SiO}_2$  (60 %),  $\text{Al}_2\text{O}_3$  (20 %), and  $\text{K}_2\text{O}$  (10 %). Approximately 84 % of the total carbon is graphite, whereas 16 % is graphitised carbon, which can be upgraded by froth flotation and acid leaching. Although the crystallinity and microcrystal structure of the graphite require further investigation, the preliminary mineralogical features meet the international standards for high-grade fine-flake graphite and suggest its suitability for advanced processing and exploration. These findings highlight the Nubian Desert as an important and underexplored graphite resource, necessitating expanded geological and industrial investigations to meet the growing demand for critical minerals required for sustainable energy technologies.

### Introduction

Graphite is a naturally occurring allotrope of crystalline carbon, found primarily in metamorphic and igneous rocks [1]. It exists in three commercial forms: crystalline lump or vein graphite, crystalline flake graphite, and microcrystalline or amorphous graphite [2]. Graphite consists of carbon atoms arranged in hexagonal layers called graphene, linked by covalent and metallic bonds via  $sp^2$

\* Corresponding author.

E-mail address: [dalaldesouqi@gmail.com](mailto:dalaldesouqi@gmail.com) (D. Desouqi).

<https://doi.org/10.1016/j.sciaf.2025.e02602>

Received 14 November 2024; Received in revised form 30 January 2025; Accepted 19 February 2025

Available online 27 February 2025

2468-2276/© 2025 The Author(s). Published by Elsevier B.V. This is an open access article under the CC BY license (<http://creativecommons.org/licenses/by/4.0/>).

hybridisation. The graphene layers are linked by weak van der Waals forces, enabling them to slide past each other easily. This unique structure provides graphite with expectational properties, including softness, lubricating ability, and excellent thermal and electrical conductivities [3].

The increasing global demand for natural graphite, driven by its crucial role in green energy transition, particularly for use in battery anodes in lithium-ion batteries, stationary batteries, lead-acid batteries, and fuel cells, has underlined the need to identify and explore new sources of natural graphite [4,5]. Recognising its importance, several countries, including the United States, China, India, and the European Union, have listed natural graphite as a critical mineral. In 2022, China produced 62 % of the global graphite, followed by Mozambique, Madagascar, Brazil, and India [6].

Given the importance of graphite in meeting global green energy goals, this study focussed on the Nubian Desert, Sudan, which holds notable unexplored potential for natural graphite deposits. Despite the regional geological significance, the exploration and mineralisation of natural graphite in the Nubian Desert has been disregarded, as historical attention has been focused on gold mining. This industry has deep roots, dating back over five thousand years to the ancient Nubians, who pioneered mining in the region—a legacy that has influenced resource extraction in Sudan to this day [7]. Conversely, neighbouring countries, such as Ethiopia and Egypt, have conducted studies on the mineralogy and processing of natural graphite, providing a detailed understanding of their graphite and graphite-bearing rocks [8,9]. Similar studies have not yet been conducted in the Nubian Desert, Sudan, leaving a significant knowledge gap regarding the graphite resources of the region. This study aimed to fill these gaps by providing a detailed investigation of rock petrographic and mineralogical analysis, including rock microtexture, graphite flake size, mineralogical composition, associated minerals, graphite carbon content, and graphite structure for graphite-bearing rocks in the Nubian Desert, lower Wadi Gabgaba in the Red Sea State, Sudan, using petrography, scanning electron microscopy (SEM), energy-dispersive X-ray spectrometry (EDX), X-ray diffraction (XRD), and thermogravimetric analysis (TGA). We supported the mineralogical characterisation by reviewing the geology of the study area. We selected this methodology because the relationship between minerals and rocks is often analysed using a mineralogical and petrographic approach [10]. We analysed our results for each technique with respect to the graphite grade and its relation to the host-rock metamorphic grade. This study establishes a foundational understanding of the graphite resources in the Nubian desert, Sudan and highlights their potential for supporting the local economy and meeting global demands. The findings of this study are particularly relevant to the growing green energy sector because graphite is crucial for manufacturing advanced battery technologies and other energy storage solutions. The insights of this study will contribute to the identification of new sources of natural graphite, support the global transition to clean energy, and provide preliminary data for future exploration and industrial applications.

### Geography and geology of the study area

The study area (Nubian Desert lower Wadi Gabgaba in the Red Sea State, Sudan) is located approximately 190 km east of Wadi

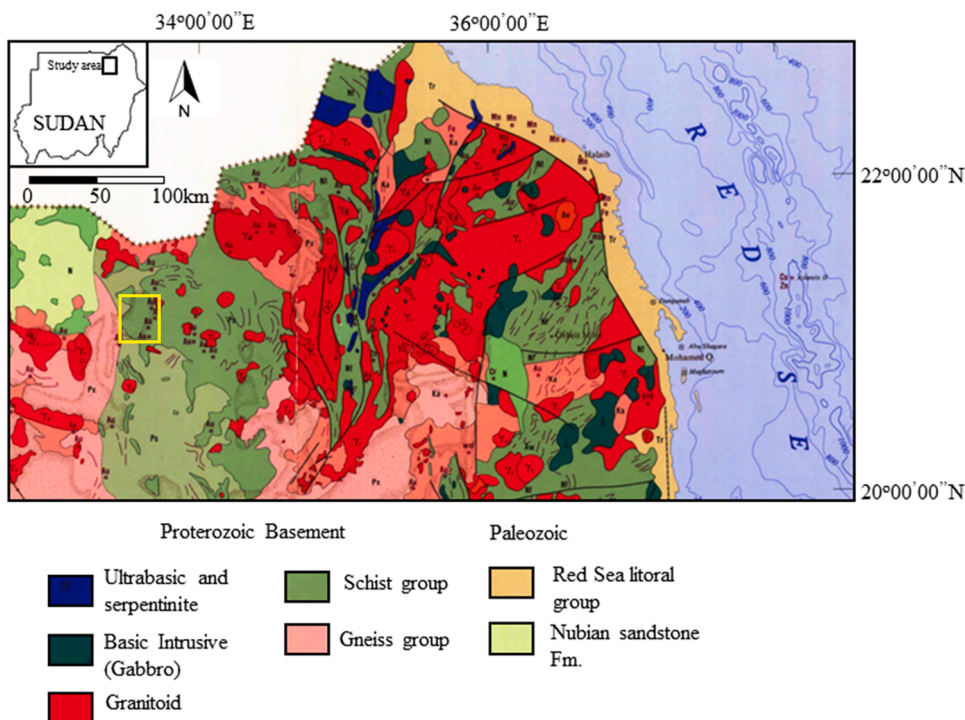


Fig. 1. Geological Map of North Sudan. The area marked by the yellow box is the study area, and that is part of the Nubian Desert.

Halfa and is situated beside the infamous ancient Nile River (latitude: 21°30'30.9"N and 33°35'54.6"W) (Fig. 1), covering an area of approximately 15 km<sup>2</sup>. The climate of the area varies from hot summers to cold winters, with extremely low humidity throughout the year. Rainfall is extremely low and vegetation growth is extremely sparse. The topography varies from 100 m above the average sea level in the lowlands to 700 m above the average sea level in the hilly areas. No rivers or drainage systems are present in the study area. Active gold mines are located in the hilly area in the eastern part of the study area.

Northern Sudan contains exposed Precambrian basement complex rocks from the Wadi Halfa of the Nile River to the eastern region of the Red Sea. The basement complex is composed of gneiss and schist, with the former showing granulite-amphibolite metamorphic facies and the latter showing amphibolite-greenschist metamorphic facies. The relative age of the gneiss group is Early Proterozoic, whereas that of the schist group is Late Proterozoic. The gneiss group is composed of granitic gneiss, magmatic, A-type granite, amphibolites, and pyroxene granulites. The schist group is dominated by mica schist, graphite, quartzite, and marble [7].

The geology of the study area consists mainly of mica graphite schist and graphite schist from the schist group of Kurmut Series [11] (Fig. S1, Supplementary Material.docx). The schist group was intruded by unfoliated stock bodies of granite, granodiorite, gabbro, and syenite dated from the Late Precambrian to Early Palaeozoic during the Pan-African orogeny [11,12]. Additionally, the presence of alkali granite is related to plate rifting during the late Pan-African orogeny [12]. The western part of the study area contains the Oolitic Ironstone Formation [13].

## Materials and methods

### Samples

Rock samples were collected from the study area, using the grab method from several trenches across the orebody. Ten samples (Fig. S2, supplementary Material.docx) were shipped to Malaysia after obtaining official authorisation from the Sudanese Ministry of Minerals. The rock samples exhibited a dark grey colour and a metallic lustre, and they left a grey trace on hands. The rocks could be scratched with fingernails, were brittle, and softer than silica (glass), measuring approximately 3 according to the standard Mohs Scale of Hardness (Fig. S3, Supplementary Material).

Polished thin sections were prepared for thin-section petrographic microscopy analysis as previously described [14]. Thin-section preparation was conducted in the optical lab and rock crushing, rock cutting, and lapidary room of the Department of Geology, Faculty of Science, Universiti Malaya. Two thin sections (30 µm thick) were prepared for petrographic observations.

EDX, SEM, XRD, TGA, froth flotation, and acid leaching were performed on a powdered rock sample in the rock crushing, rock cutting, and lapidary room of the Department of Geology, Faculty of Science, Universiti Malaya. The powdered rock sample was earthy grey in colour and prepared by crushing, milling, and sieving of eight rock samples into various fraction size fractions (-150, -212 + 150, -300 + 212, -425 + 300, -600+425,+600 µm) [15]. The particles were ground further to < 5 µm prior to EDX, SEM and XRD analyses. For TGA, the pure rock and upgraded samples size fractions were ground to < 150 µm.

The samples used for EDX and SEM were dispersed in the diesel phase to form a suspension for increased carbon detection. The graphite residue sample was washed and dried overnight in an oven at 110 °C. We performed dispersion rather than dissolution to prevent the reduction in the associated minerals and total carbon content [16,17].

### Bench scale froth flotation and acid leaching

Rock samples were subjected to initial bench-scale froth flotation trials as described by [24], using various size fractions: (-150, -212 + 150, -300 + 212, -425 + 300, -600+425,+600 µm). Among these, the (-300 + 212 µm) size fraction produced the highest ratio of concentration (Fig. S7, supplementary material.docx); therefore, froth flotation was subsequently conducted using this fraction (-300 + 212 µm). Pine oil was used as a frother, kerosene oil as a collector, sodium metasilicate (Na<sub>2</sub>SiO<sub>3</sub>) as a depressant, and sodium carbonate (Na<sub>2</sub>CO<sub>3</sub>) as a pH adjuster to pH 7.5. The froth flotation concentrate was washed and dried overnight in an oven at 60 °C. To eliminate silica and alumina, the dried sample concentrate was digested using 100 % concentrated hydrofluoric acid (AR grade, 49 %; Riedemann-Schmidt). The solid residue was washed, neutralised with distilled water, filtered, and dried for 48 h at 26 °C. Leaching was performed at room temperature with a solid-to-liquid ratio of 1:5, stirring speed of 700 rpm, and duration of 2 h. The experimental details of the acid leaching with safety precautions are described (Method M1; Fig. S4, supplementary material.docx).

### Analytical techniques

The petrographic observations were conducted using a standard procedure [14] that utilised both X-Nicol and plane-polarised light. The magnification used to capture the photomicrographs was 100 × because of the fine-grained size yield of the sample. Photomicrographs were captured under an ordinary white light bulb (no other kind of light was used).

Surface morphology and microstructural analyses were conducted in the material characterisation laboratory of the Universiti Putra Malaysia, using a Hitachi S-3400 N scanning electron microscope operated in high-vacuum mode with an accelerating voltage of 20 kV, working distance of 5.2 mm, and secondary electron (SE) imaging mode. Images were captured at 1000 × and 3000 × magnifications.

Elemental analysis was performed using EDX Thermo Scientific (model Noran) at the Material Characterization Laboratory, Universiti Putra Malaysia. A standard SEM holder made of aluminium and covered with carbon tape was used to minimise the potential of false signals, which could affect the accuracy of the measurements for aluminium and carbon, and the sample was coated with

platinum. A conductive coating can enhance X-ray signals, making it easier to identify and quantify the elemental composition of the sample [18]. EDX was selected for general chemical analysis rather than advanced techniques, such as inductively coupled plasma mass spectrometry (ICP-MS) and X-ray fluorescence (XRF) because of its cost-effectiveness, user-friendliness, and simple sample preparation [19,20].

The powder XRD patterns of the rock sample were conducted in the material characterisation laboratory of the Universiti Putra Malaysia, using an X-ray diffractometer (XRD 6000; Shimadzu) with a characteristic X-ray  $\text{CuK}\alpha$  radiation (wavelength  $\lambda = 1.5406 \text{ \AA}$ ) that was generated from an X-ray tube (target = Cu, voltage = 40.0 kV, and current = 30.0 mA). The X-rays diffracted from the sample were controlled by a divergence slit ( $1.00000^\circ$ ), reduced by a scatter slit of  $1.00000^\circ$ , and received by a receiving slit of  $0.30000 \text{ mm}$ . The scanning measurement conditions were drive axis =  $\theta - 2\theta$ , scan range =  $10.000\text{--}60.000^\circ$ , scan mode = continuous scan, scan speed =  $2.0000^\circ$  per min, sampling pitch =  $0.0200^\circ$ , and preset time = 0.6 s.

TGA was conducted on three samples: pure rock, upgraded rock obtained through froth flotation, and upgraded rock obtained through acid leaching. The respective sample weights were 20.063, 10.877, and 2.483 mg, with all samples ground to a particle size of  $<150 \text{ }\mu\text{m}$ . TGA was performed using a Mettler Toledo instrument (TGA-DSC HT 3). The heating rate was  $10^\circ \text{C}/\text{min}$  within a temperature range of  $25\text{--}1100^\circ \text{C}$  under a constant oxygen atmosphere ( $50 \text{ ml}/\text{min}$ ). The quantitative analysis of the thermally active minerals was based on the stoichiometric factors of the involved reactions [21]. TGA was performed in an oxygen atmosphere rather than air, as the carbon oxidises almost completely in the oxygen atmosphere, whereas it only oxidises partially in the air atmosphere,

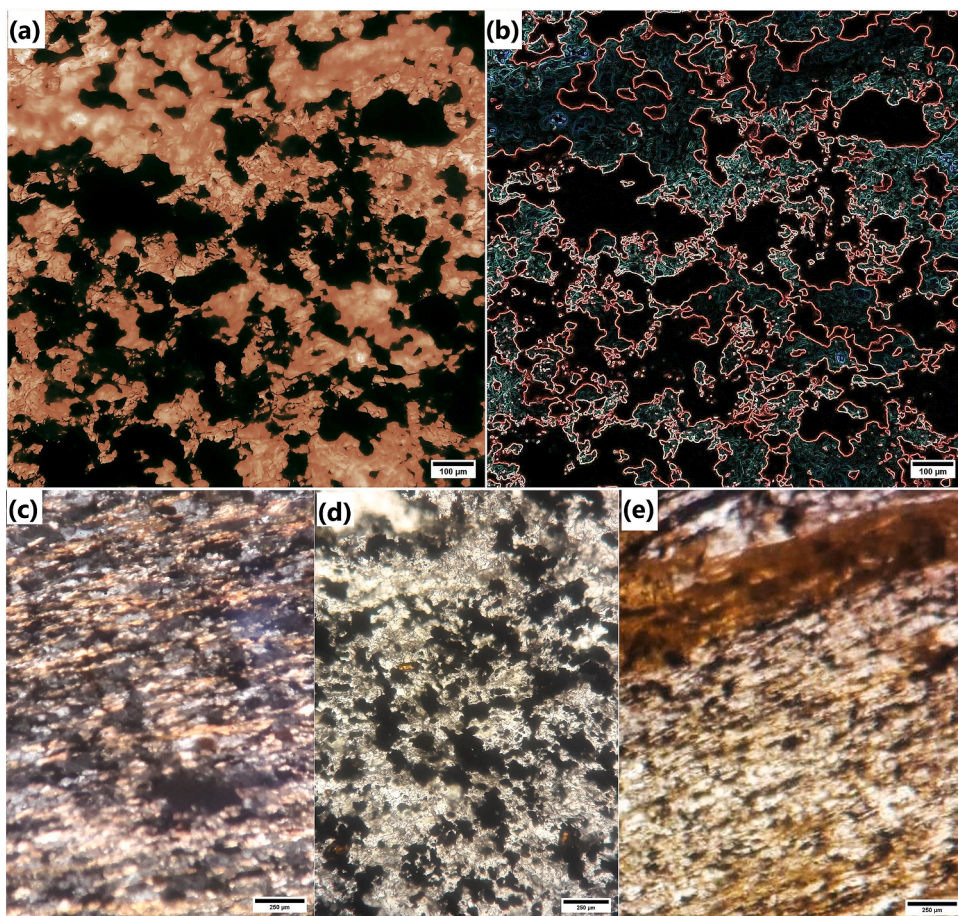


**Fig. 2.** The photomicrographs illustrate the mineralogical textures and foliation patterns of the fine-grained Nubian desert graphite schist rock sample: (a) The dark black segmented regions represents graphite flakes, finely disseminated and aligned within the schist matrix. The lighter areas represent silicate minerals namely quartz and minor feldspars, with reddish-brown tones corresponding to mica (biotite or muscovite). (b) Foliation is highlighted by segmented red outlines, tracing the alignment of graphite and silicate minerals, emphasizing the parallel to sub-parallel structure within the schist rock matrix. (c) A finer-grained with distinct foliation texture under cross-polarized light, showcasing black graphite, brownish and golden tones of mica alongside translucent to pale gray quartz and feldspar grains. (d) The mineral assemblage appears dominated by black graphite in fine-grained forms, interspersed with lighter gray to whitish feldspar and quartz grains. (e) A transition zone between mineral phases, highlighting the dark black graphite lamellae intergrown with golden-brown mica and lighter silicates, showing well-defined foliation. Overall, the rock sample displays a prominent foliated texture, defined by the alignment of graphite and silicate minerals, with graphite presenting as black, flaky grains and the other minerals exhibiting distinct optical properties under polarized microscope.

resulting in better quantification of the carbon material; however, the oxygen atmosphere could destroy the sample holder more rapidly [22]. TGA was conducted in the characterisation laboratory at the Institute of Advanced Technology, Universiti Putra, Malaysia. TGA was prioritised for this study because of its ability to provide precise quantitative data on the thermal stability and graphitic carbon content of graphite-bearing rocks, which are essential for evaluating the graphitic carbon content. Additionally, TGA helps in understanding the metamorphic temperature conditions by analysing the thermal behaviour of rocks. In graphite-bearing rocks, the exothermic reactions of carbon provide key insights into the metamorphic grade of the rocks, indicating the temperature conditions during their formation [23,24]. Although Raman spectroscopy is highly effective for assessing crystallinity and deriving peak metamorphic temperatures, it was not initially used because our study prioritised broad mineralogical and chemical characterisations over structural analysis [23,25,26].

Petrographic photomicrographs were analysed and segmented using ImageJ software (ImageJ; National Institutes of Health, Bethesda, MD, USA) and Adobe Photoshop (Adobe Inc., San Jose, CA, USA). The initial crystal-phase identification of the collected powder XRD pattern was conducted using Profex software (Profex; University of Göttingen, Göttingen, Germany), whereas the phase quantitative analysis was conducted using MAUD software (MAUD; University of Parma, Parma, Italy) using  $\text{CuK}\alpha$  X-ray instrument standard parameters and the American Mineralogist database. The refinement data were collected using the Bragg-Brentano geometry. The XRD and TGA graphs were obtained using Origin Pro software (OriginPro; OriginLab Corporation, Northampton, MA, USA).

## Results and discussion

### Petrography

Petrography was used to identify mineral composition, analyse rock texture, and classify the rock sample. The Nubian Desert graphite schist is primarily composed of graphite, quartz, mica muscovite, and mica biotite. These minerals are fine-grained and sorted into parallel to subparallel alignment foliation textures (Fig. 2). One rock sample exhibited weak schistosity (Fig. 2a and d), whereas the other exhibited strong schistosity (Fig. 2c and e).

The graphite flakes appeared black (opaque) when rotated under plane-polarised and X-Nicol light and present as disseminated carbonaceous materials. The graphite crystals are irregular elongated or round flakes and were present in orientations parallel and subparallel to the schistosity along the quartz and feldspar grain boundaries. The coarse graphite flakes are fine, ranging from 50 to 150  $\mu\text{m}$  in length (Fig. S5, Supplementary Material). However, extremely fine flakes below 50  $\mu\text{m}$  are also present, as medium flakes are ranging from 200 to 500  $\mu\text{m}$  in length. Graphite accounts for approximately 10 % of the rock sample by volume rocks. The average graphite flakes width is 46  $\mu\text{m}$  (Fig. 2).

Quartz and feldspar exhibited a light-to-dark grey when rotated under X-Nicol light (Fig. 2). The quartz formed an anhedral crystal shape and exhibited undulatory (wavy) extinction. The quartz grains are anhedral in shape and size less than 200  $\mu\text{m}$  in length; in addition, smaller grains of < 100  $\mu\text{m}$  exist that are likely feldspar [27]. Quartz is less abundant in the biotite-rich areas of the thin sections. Quartz accounts for approximately 40–45 % of the rock sample by volume.

Mica (muscovite and biotite) are present in parallel and subparallel directions along the schist foliation. Biotite exhibited significant pleochroism, whereas it was absent in muscovite. Mica exhibited a platy crystal habit and several mica grains were observed in detail using a polarized microscope, exhibiting a perfect set of cleavages parallel to 001 or along the C-axis. The mica flakes are elongated platy that aligned to form foliations along with graphite. Mica accounts for approximately 45–50 % of the rock sample by volume. The muscovite crystals are irregular thin flakes in shape and size and are < 300  $\mu\text{m}$  in length. Muscovite is more abundant than biotite in the rock sample. The biotite grains are platy and 110–386  $\mu\text{m}$  in diameter. In the biotite-rich areas, all quartz was extinct, whereas most of the muscovite is grown into biotite (Fig. 2). All crystals are larger relatively including graphite, in the thin section which exhibited strong schistosity (Fig. 2c and e). Graphite and mica are probably the source of the dark grey colour of the rock sample (Fig. S3, Supplementary Material). Moreover, we were unable to confirm the absence of hematite in thin sections using this technique.

The study area contains at least three types of schist: graphite, quartz mica, and muscovite graphite [28]. The dissemination and irregular shape of opaque carbonaceous material (CM) flakes with parallel alignment along the schist foliation observed by petrography (Fig. 2), are typical features of graphite of organic origin in an increasing metamorphic environment [29]. The origin of the graphite can be better understood using carbon isotope analysis and infrared (IR) spectroscopy [30]. Based on the natural graphite classification with respect to the flake length and the rock formation environment [1,31], the petrography results indicated that the natural graphite of the Nubian Desert graphite schist was probably formed in an increasing regional metamorphic environment as a fine flake graphite with flake lengths of 50–150  $\mu\text{m}$  and an average width of 46  $\mu\text{m}$  (Fig. 2).

The absence of graphite where quartz is present (Fig. 2) was also observed by [32]. The relationship between the dispersion of graphite flakes and quartz grains can be better understood by studying the rock formation mechanisms [33]. Additionally, the lower abundance of quartz grains in biotite-rich areas (Fig. 2) indicates the recrystallisation and deformation of metamorphic rocks in an increasing metamorphic environment [34]. Consequently, the graphite-mica schist could have been subjected to increasing metamorphic conditions sufficient for recrystallisation. Additionally, the existence of quite longer graphite flakes in the strong schistosity rock sample areas of the thin sections (Fig. 2c and e) may have occurred because of the increasing metamorphic grade of the graphite mica schist [35]. This phenomenon supports the increasing metamorphic grade of the Nubian Desert graphite schist rock and encourages the exploration of strong schistosity zones in the study area for larger crystalline flake graphite deposits. The presence of these index minerals in the Nubian Desert graphite schist rock sample also indicates the increasing regional metamorphism of high-grade amphibolite-to-green schist facies.

### Scanning electron microscope (SEM)

SEM was conducted to further investigate the morphology and size distribution of the minerals in the rock samples. The SEM images revealed a predominance of flake-like particles with varying sizes and morphologies (Fig. 3). Larger, intact flakes displayed a characteristic layered structure, confirming the presence of minerals, such as graphite and mica, both of which exhibit basal cleavage. The morphology and distribution of these flakes suggested that the rock sample underwent metamorphism, during which graphite and mica were probably formed or recrystallised under high temperature and pressures. In addition to the flaky minerals, interspersed angular and non-flaky particles were identified as quartz or other non-layered impurities. The edges of the flakes are irregular with visible signs of breakage, probably resulting from grinding during sample preparation. The surface textures range from smooth to rough with smaller debris particles adhering to larger flakes. These rough surfaces and fragmented edges suggested exfoliation of layered minerals, particularly graphite and mica, during grinding and sample preparation. SEM analysis confirmed the mineralogical composition and metamorphic origin of the Nubian Desert graphite schist sample.

### Elemental analysis by energy-dispersive X-ray spectrometry (EDX)

EDX was used to perform quantitative elemental analysis of the rock samples (Table 1) (Fig. S6, Supplementary Material).

Generally, organic carbon/ CM in regional metamorphic environments transform into less-ordered graphitised carbon and fully ordered crystalline graphite with increasing temperature and moderate-to-high pressure [36]. According to [1], the carbon content of metamorphic graphite is approximately 70 % for microcrystalline graphite, that is more often found in contact metamorphic regions, whereas the carbon content of crystalline flake graphite varies between 2 and 30 % and is found most often in regional metamorphic environments. We assumed that the elemental carbon detected in the rock samples was graphite or a form of carbonaceous material (CM) in the metamorphic rocks (Table 1). Based on petrographic observations, the graphite of the Nubian Desert Graphite Schist rock is probably fine flake graphite and the environment of the rock sample collection is expected to be an increasing regional metamorphic

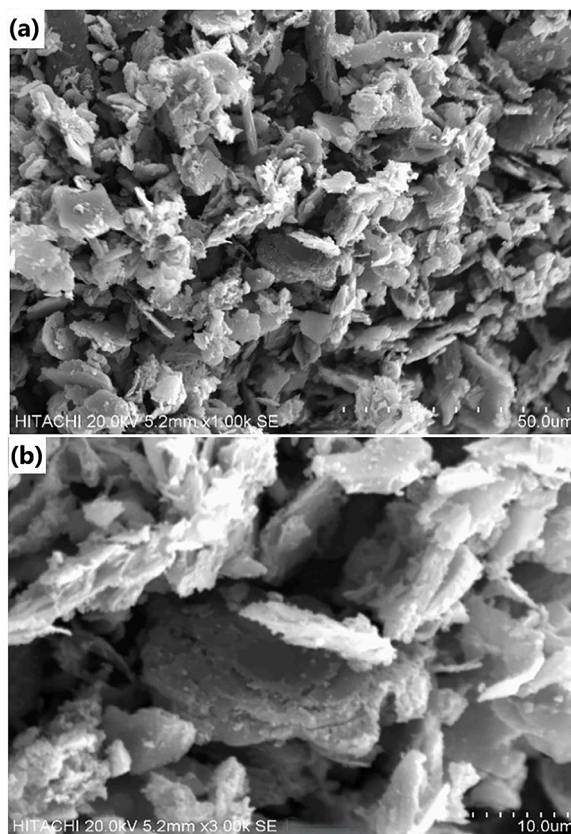


**Fig. 3.** SEM images of a mineral mixture containing graphite, mica, and quartz showing their foliated and flaky structures. (a) A broad view of the sample highlighting the overall foliated texture characteristic of mica and graphite, interspersed with quartz particles. The parallel alignment of the platy minerals (graphite and mica) demonstrates their foliated nature. (b) A closer view displaying individual flaky features of the graphite and mica. The largest mineral observed in this image is graphite, identifiable by its darker appearance compared to the other particles, owing to its lower atomic number. Graphite exhibits sheet-like morphology, further emphasizing its cleavage and layered structure. Quartz grains appear irregular and embedded within the foliated matrix.

**Table 1**  
Quantitative elemental analysis of the Nubian Desert graphite rock based on EDX.

Element	Atomic%	Weight%	Formula	Compound%
C	11.48	19.27	C	11.48
O	40.69	51.31	...	...
Al	11.02	8.24	Al <sub>2</sub> O <sub>3</sub>	20.81
Si	27.11	19.48	SiO <sub>2</sub>	58.01
K	9.70	1.71	K <sub>2</sub> O	9.70
Total	100	100		100

environment. Correspondingly, the elemental carbon detected by EDX is probably a mixture of less-ordered graphitised carbon and fully ordered crystallised graphite. Additionally, the carbon content (10 %) of the Nubian Desert graphite schist (Table 1), indicates that the schist could have been subjected to regional metamorphism, and the crystallised natural graphite of the rock sample is probably flake crystalline graphite. Although the EDX instrument sample holder and sample dispersion in diesel may have influenced the elemental analysis, the graphite content estimated by TGA for the rock sample upgraded with froth flotation was approximately 12 %, supporting the accuracy of EDX. Additionally, the petrographic analysis of graphite was 10 % by volume and approximately 8.3 % by wt.%, assuming the schist matrix density is 2.7g/cm<sup>3</sup> [37].

The presence of Fe in the rock sample is shown in (Fig. S6 Supplementary Material), supporting the presence of mica biotite in the rock sample. However, the quantity of Fe/Fe<sub>2</sub>O<sub>3</sub> was not detected (Table 1). Trace and variable elements, such as Ti, Mn, Mg, Ca, and Na are often found in micas [38]; they were not detected using EDX. Because this study focused on major elemental analysis and had a limited budget, we recommend that future studies utilise advanced techniques, such as inductively coupled plasma mass spectrometry (ICP-MS or X-ray fluorescence (XRF, for comprehensive chemical composition analysis, including trace elements [20].

The composition of micas with a reasonable amount of K, as in the Nubian Desert rock sample, reveals that the chemical reaction was an open system during metamorphism [39]. An open system is necessary for the formation of overgrowth and muscovite, replacing K-feldspar and quartz, because both have similar chemical compositions. Therefore, mica could have recrystallised during metamorphism from the existing quartz and feldspar in the parent rock, along with an existing carbon source. Additionally, significant contents of Al<sub>2</sub>O<sub>3</sub> and K<sub>2</sub>O have been observed with an increase in graphite content and low Fe<sub>2</sub>O<sub>3</sub> [32,40]. A relatively high Fe<sub>2</sub>O<sub>3</sub> in the reaction system could reduce graphite to zero retrograde (decreasing metamorphism). Accordingly, the Nubian Desert graphite schist may have been subjected to an increasing metamorphic environment, where feldspar was replaced by mica muscovite and carbon was graphitised.

#### Crystallinity from X-ray crystallography (XRD)

XRD was used to investigate the crystalline phases and bulk chemical compositions of the rock samples. The bulk mineralogy determined by XRD showed that the rock sample composed primarily of mica muscovite 2M-1 (50 %), quartz (44 %), graphite, albite (5

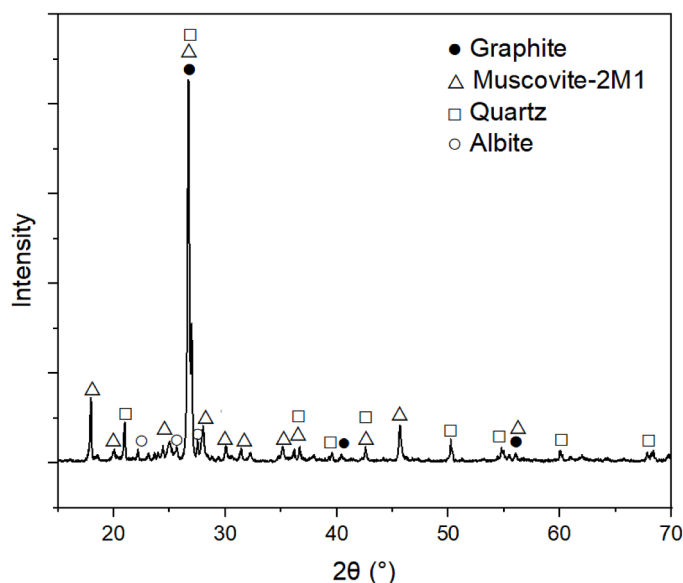


**Fig. 4.** X-ray diffraction pattern of rock sample. Graphite Characteristic peak; at  $2\theta \approx 26.73^\circ$  for (d0 0 2 / d0 0 3) plane reflex is overlapping with characteristic peaks of both Muscovite 2M1; at  $2\theta \approx 25.52^\circ$ ,  $26.65^\circ$ , and  $26.82^\circ$  for (d-1 1 4), (d 0 2 4), and (d0 0 6) plane reflexes, and quartz peak; at  $2\theta \approx 26.63^\circ$  for (d0 1 1) and (d1 0 1) plane reflexes.

%), and trace amounts of kaolinite (Fig. 4). We assumed that both natural crystal phases of graphite, namely, hexagonal (2H) and rhombohedral (3R), to be present in the rock sample. The graphite quantity determination could not be determined by Rietveld refinement because the graphite 2H/3R characteristic peak at  $2\theta \approx 26.73^\circ$  for the (d0 0 2 / d0 0 3) plane reflexes overlapped the characteristic peaks of Muscovite 2M-1 at  $2\theta \approx 25.52^\circ$ ,  $26.65^\circ$ , and  $26.82^\circ$  for the (d-1 1 4), (d 0 2 4), and (d0 0 6) plane reflexes and quartz at  $2\theta \approx 26.63^\circ$  for the (d0 1 1) and (d1 0 1) plane reflexes. The minimum Rb (%) factor obtained after Rietveld refinement using Maud software was 25.14. Owing to the complexity of multi-phase refinement, this factor could not be reduced; thus, we could not enhance the determination of the graphite phase. Owing to a lack of funds, we could not perform a crystallographic analysis of an upgraded rock sample by froth flotation and acid leaching (40 % carbon) (Fig. 5), that could have resulted in better crystallographic analysis of the graphite phase. Biotite was not detected in the XRD pattern (Fig. 4), although it was detected by petrography. However, owing to the characteristic sequence similarity between biotite and muscovite [41], the sorting of biotite from the muscovite in the XRD pattern was not possible. According to [42], a reduction in asymmetry in the low-angle diffraction peaks of biotite can enhance its detection. Albite is a feldspar mineral present in approximately 5 % of the rock samples. The presence of albite determined by XRD explains the appearance of feldspar with optical analysis by petrography (Fig. 2).

Graphite and fine-grained dispersed CM structures in metamorphic rocks range from virtually amorphous to fully crystalline. The crystallinity perfection increases with the grade of metamorphism. Fully ordered graphite first appears in the uppermost grade greenschist facies to lower amphibolite facies with increasing temperature (300–500 °C) and pressure ( $P \geq 3$  kbar), whereas less ordered graphite could be formed by the extremes of total pressure [43,44]. Hexagonal graphite (2H) with the ABABAB... stacking sequence of graphene layers is the most commonly found crystal form. The rhombohedral form of graphite (3R) with a stacking sequence of ABCABC... is a minor component of well-crystallized graphite [3]. The XRD results of the Nubian Desert rock sample showed that the characteristic graphite peak overlaps with the characteristic peaks of muscovite 2M-1 and quartz (Fig. 4). According to the petrography and SEM graphite present in the rock sample and according to EDX elemental analysis, carbon is present. Additionally, based on petrography and EDX, the graphite mica schist probably metamorphosed in a regional metamorphic environment. Based on the XRD results, we can assume that the Nubian Desert flake graphite has a mixed structure of fully ordered crystalline graphite and semi-ordered graphitised carbon (2H /3R) (Fig. 4). However, owing to the complexity of defining the graphite crystal pattern of the Nubian Desert flake graphite in the presence of abundant muscovite and quartz crystals, estimating the graphite content and microstructure estimation by XRD and Rietveld refinement is challenging (Fig. 4). The technological application and accurate categorisation of graphite (fully ordered) from graphitised carbon (semi-graphite/less-ordered) depend on the precise microstructure of the graphite crystals, particularly the interplanar spacing ( $\text{\AA}$ ) d0 0 2 planes and that is in case of hexagonal phase (2H) = (3.349–3.354  $\text{\AA}$ ), crystallite size  $L_c$  0 0 2 ( $\text{\AA}$ ), and lattice parameters ( $a_0 = b_0 = 2.464 \text{\AA}$ ,  $c_0 = 6.711 \text{\AA}$ ). We can overcome this limitation in our future study by separating graphite with froth flotation and acid leaching (100 % C), followed by characterisation of the graphite microstructure and degree of graphitisation by XRD, Raman spectroscopy, and transmission electron microscopy (TEM) [45–47].

Muscovite 2M1 is a high-grade crystal phase and in regional metamorphic environments, it is most common during increasing metamorphism (prograde) [48]. Moreover, muscovite (M1) usually occurs as a 2M polymorph in the carbon-rich zones of the regional

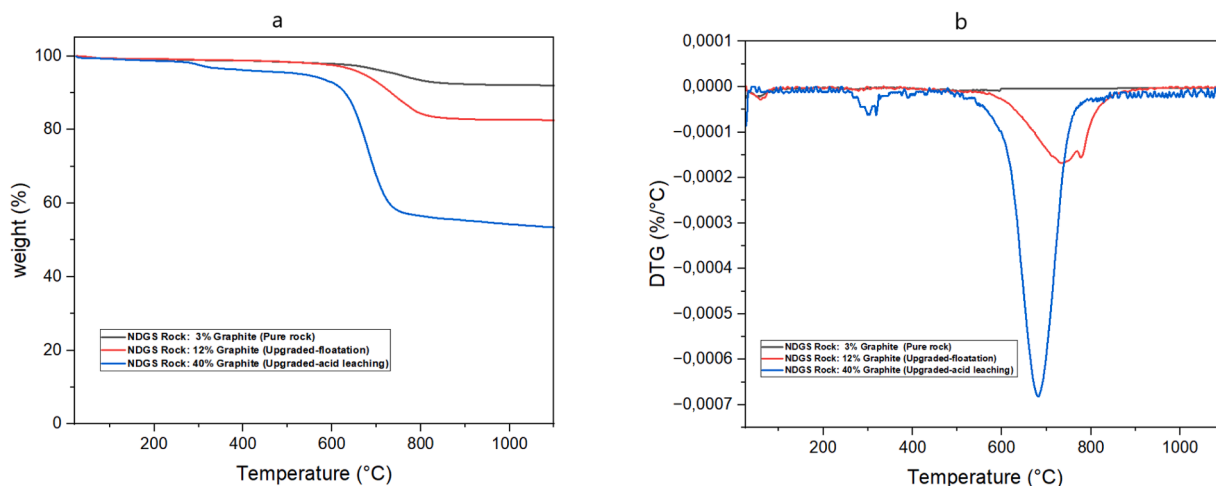


**Fig. 5.** Thermogravimetric Analysis (TGA) and Derivative Thermogravimetry (DTG) curves of NDGS (Nubian Desert Graphite Schist) rock samples showing weight loss and thermal decomposition. (a) TGA curves display weight (%) loss with increasing temperature: 3 % Graphite (Pure rock): Modest weight loss due to the overlapping decomposition of mica muscovite and graphite. 12 % Graphite (Upgraded-floatation): More pronounced weight loss, still showing mica-graphite overlap. 40 % Graphite (Upgraded-acid leaching): Dramatic weight loss due to high graphite content with no mica muscovite overlap. (b) DTG curves show derivative weight loss (%/°C): The first two samples (3 % and 12 % Graphite) exhibit overlapping mica and graphite peaks. The third sample (40 % Graphite) shows a distinct graphite peak with minimal mica muscovite influence. The exothermic DTG peaks of graphite in the three samples, indicate the metamorphic grade, with higher graphite crystallinity reflecting greater thermal stability. The graphitized carbon exothermic effect in the 3 % Graphite pure rock sample suggests a mixed structure with semi and well-ordered carbon phases.

metamorphic environment [48]. The presence of muscovite 2M1 in the rock sample, based on XRD (Fig. 4) and in agreement with petrography and EDX, indicates that the Nubian Desert graphite schist was metamorphosed in an increasing regional metamorphic environment.

#### *Thermal analysis using thermogravimetric analysis TGA*

TGA was used to examine the exothermic and endothermic effects as well as the carbon content of the pure rock, upgraded rock with froth flotation, and upgraded rock with acid leaching. Graphite oxidises in an exothermic reaction, leading to a mass change during thermogravimetric (TG) and derivative thermogravimetric (DTG) analyses under an oxygen atmosphere and a constant heat rate from 25 to 1100 °C [49]. The DTG peak indicated the temperature at which the maximum rate of mass loss occurred (Fig. 5). Using stoichiometric factors, the content of the thermally active minerals in the samples was estimated. The key temperature ranges, corresponding DTG peaks, mass losses, and relevant references are summarised in (Table S1 . Supplementary Material.docx) The exothermic effect of graphite and the associated mass loss in all three samples confirmed the presence of graphite and its transformation during oxidation. The graphite content of the pure rock sample and upgraded sample with froth flotation may be slightly underestimated. Uncertainties of approximately  $\pm 3$  % (Table S1, Supplementary Material) in the content of graphite and mica muscovite arise from the potential overlap between the carbon oxide gases (CO and CO<sub>2</sub>) released during the exothermic reaction of graphite and the water vapor released during muscovite dihydroxylation (Fig. 5), as well as measurement variability, particle size, applied atmosphere, phase transitions, and instrumental limitations. These factors can affect the interpretation of TGA results when compared to petrography and EDX. However, an overlapping effect was not observed in the rock sample upgraded with acid leaching owing to the decrease in muscovite content and the drastic increase in graphite content (Fig. 5).

Graphite oxidises in the presence of oxygen at high temperatures, typically in the range of 400–800 °C [50,51]. In metamorphic rocks, graphite can be mixed with graphitised carbon [51–53]. As the temperature and time increase, the rock metamorphism grade, crystallinity of graphite, and graphite content of the metamorphic rocks also increase [44]. Moreover, the exothermic effect of graphite-bearing rock peak of different metamorphic facies is: (a) greenschist facies (500–640 °C); (b) amphibolite facies (640–800 °C); and (c) granulite facies (above 800 °C) [51]. The TGA results showed that the graphite in all three samples underwent an exothermic oxidation reaction, resulting in a noticeable mass loss within the temperature range characteristic of graphite oxidation. (Fig. 5) (Table S1, Supplementary Material). The presence of graphite in the pure rock and samples upgraded by froth flotation and acid leaching was confirmed by the exothermic peak typical for graphite oxidation in the DTG curve (Table S1, Supplementary Material.docx). The two-step oxidation of graphitised carbon in the rock sample indicated its minor contribution compared to that of graphite, highlighting the distinct graphite behaviour in TGA. This distinction is evident in the drastic exothermic behaviour of graphite observed in the upgraded graphite sample (Fig. 5). These results indicate the presence of carbon in the Nubian Desert graphite rock as a mixed structure of fully ordered graphite (2H/3R) and less-ordered graphitised carbon, with the graphite content being significantly higher than that of graphitised carbon (Table S1, Supplementary Material). Additionally, the temperature of the graphite exothermic effect peak is characteristic of the metamorphic temperature of graphite or graphite-bearing rock samples [49]. These temperatures were measured at 695.52 °C in the Nubian Desert rock sample (pure), 727 °C in the upgraded sample with froth flotation, and 677.05 °C in the upgraded sample with acid leaching. In agreement with the petrographic analysis, these prominent peaks highlight that, the Nubian Desert graphite schist has been subjected to the increasing metamorphism of high-grade amphibolite-to-green schist facies. However, a more accurate metamorphism (graphitisation temperature) could be determined after the separation of graphite (pure carbon 100 % C).

We suggest that the abundance of the mica phase in the Nubian Desert graphite-schist sample caused its overlap with the graphite in the rock sample [49,26]. The abundance of mica was confirmed using petrography, SEM, and XRD. However, an overlapping effect was not observed in the upgraded sample with acid leaching because most of the mica had dissolved. Moreover, an increase in mica content in the upgraded sample with froth flotation suggested that mica muscovite could float with graphite owing to their similar hydrophobicity. Despite the limitations of TGA, the method proved sufficient for detecting and quantifying the graphite phase and the expected peak metamorphism. The oxidation properties of the coal samples characterised by the exothermic effect indexes were found to be similar to those of the Raman band area ratio effect [23]. However, the future integration of Raman spectroscopy with TGA will offer complementary insights, enhancing our understanding of the crystallinity, geological history, and industrial potential of the graphite. If TGA is selected for such an analysis, the absence of quartz and albite phase transitions in the TGA profile could be enhanced using complementary techniques, such as differential scanning calorimetry (DSC) to achieve broader phase identification in future studies [48]. Moreover, the muscovite dehydroxylation reaction (DTG peak at 748.89 °C) (Fig. 5) indicated that muscovite is fine-grained [52]. Graphite and mica follow the foliation texture [34] of the Nubian Desert rock sample based on the petrographic results (Fig. 2). Therefore, muscovite dihydroxylation indicates that both graphite and mica are fine-grained within the Nubian Desert graphite schist.

#### *Influence of froth flotation and acid leaching*

The combination of froth flotation and acid leaching effectively upgraded graphite from low-grade ores [54]. In the case of Nubian Desert graphite, flotation increased the carbon content from 3 % to 12 % with a 75 % recovery rate (Table S2, Supplementary Material.docx), efficiently removing a significant portion of the gangue minerals. The effectiveness of flotation was influenced by the particle size distribution, with the -300 + 212  $\mu\text{m}$  fraction producing the most stable froth (Fig. S7), indicating a strong affinity between the graphite flakes and the hydrophobic collector. However, the entrainment of fine particles and the limited floatability of coarser flakes

likely contributed to graphite losses during this stage. Acid leaching further improved the purity, increasing the carbon content to 40 % with a 70 % recovery rate (Table S2, Supplementary Material), leading to an overall combined graphite recovery of 52.5 %. The ability of hydrofluoric acid to dissolve silicate minerals played a key role in enhancing graphite purity; however, its limitations in completely removing certain impurities, particularly residual silica and alumina, highlight the need for process optimization. The potential flotation of alumina alongside graphite could reduce the efficiency of both the flotation and leaching steps, suggesting that adjusting depressant concentrations or exploring alternative reagents may enhance selectivity. Despite these promising results, the unrecovered graphite suggests opportunities for refining the flotation and leaching conditions to improve both yield and purity. Further adjustments to frother dosage, pH control, and reagent selection could minimize impurities while maximizing graphite recovery. Additionally, the use of alternative leaching methods, such as hydrochloric acid or thermal purification, could mitigate environmental concerns associated with hydrofluoric acid while achieving comparable or superior purification efficiency [55]. These findings underscore the potential of Nubian Desert graphite as a viable resource while emphasizing the importance of continued process optimization for sustainable and efficient extraction.

## Conclusion

Based on the mineralogical and petrographic investigations of the Nubian Desert graphite schist rock, we conclude the following:

1. The Nubian Desert graphite schist is fine-grained and probably formed under high-grade metamorphic conditions with the increasing regional metamorphism of amphibolite-to-greenschist facies. The major mineral constituents of the Nubian Desert graphite schist are graphite (10 %), quartz (35 %), mica (biotite+muscovite) (50 %), and albite (5 %), whereas the quantitative elemental composition is: elemental carbon (C) (9 %), SiO<sub>2</sub> (60.79 %), Al<sub>2</sub>O<sub>3</sub> (21.7 %), and K<sub>2</sub>O (9.21 %).
2. The natural graphite in the Nubian Desert Graphite Schist rock is probably a high-grade crystalline fine flake graphite of oval and round flakes 50–150 μm in length, an average width of 46 μm, and a total carbon content of approximately 10 %. The total carbon is a mix of graphite (fully ordered) and graphitised carbon (less ordered), with fully ordered graphite (hexagonal/rhombohedral 2H/3R) accounting for approximately 84 % of the total carbon. Although the microcrystal structure of graphite is not yet clear and requires further investigation, the graphite from Nubian desert has significant potential for industrial applications, including green energy storage systems, such as lithium-ion batteries. However, beneficiation and refining processes are necessary to enhance graphite purity.
3. Fine-flake graphite is expected to become the primary source of natural graphite in the future, primarily because of the depletion of large flake graphite reserves caused by extensive mining activities. Accordingly we encourage further exploration and processing trials of the Nubian Desert flake graphite. Additionally, medium-flake graphite deposits can be discovered in areas with pronounced schistosity zones.

## Glossary

Term	Definition
Amphibolite facies	Refer to the most common <a href="#">metamorphic rocks</a> formed by <a href="#">regional metamorphism</a> under high pressure and high temperature . The amphibolites usually occur along with the mica schist and <a href="#">gneiss</a> .
Carbonaceous material (CM)	Refers to all solid, reduced, carbon materials found in sedimentary, igneous, and metamorphic rocks, including kerogen, pyrobitumen, graphitizing carbons, and crystalline graphite.
<a href="#">Contact metamorphism</a>	Is caused by <a href="#">igneous intrusions</a> as a result of the thermal effects of hot <a href="#">magma</a> on the surrounding cooler country rock. Temperatures may be up to 1000 °C at relatively low pressures (0.05–0.5 GPa). Pyrometamorphism is a special form of <a href="#">contact metamorphism</a> at very high temperatures (> 1000 °C) and very low pressures (< 0.1 GPa), affecting small fragments of country rock in a volcanic or subvolcanic environment. <a href="https://www.sciencedirect.com/topics/earth-and-planetary-sciences/regional-metamorphism">https://www.sciencedirect.com/topics/earth-and-planetary-sciences/regional-metamorphism</a> .
Foliation	Is a planar structure given by preferred orientation of minerals generally showing a platy or tabular habit. The preferred orientation is produced by deformation and is uniformly pervasive in a rock. Foliation is commonly developed in metamorphic rocks and includes cleavage, schistosity, gneissosity and gneissic
Greenschist facies	Refers to rocks which were affected by low- to medium-grade metamorphic conditions corresponding to temperatures of about 300–500 °C and pressures of 3–20 kbar, conditions equivalent to crustal depths of about 8–50 km.
Hybridization	Refers to hybrid orbital theory, where 2s and 2p carbon atomic orbitals are combined to create a set of hybrid orbitals (sp <sup>n</sup> with ρ = 3, 2, 1) that describe the chemical bonds and geometry of simple molecules
Hydrothermal origin graphite	It is proposed that carbon was mobilized from sediments as CO <sub>2</sub> and CH <sub>4</sub> during metamorphic devolatilization reactions. The carbon-bearing species were transported in aqueous fluids through hydraulic fractures.
Increasing metamorphism (prograde)	As the temperature and/or pressure increases on a body of rock we say the rock undergoes prograde metamorphism or that the grade of metamorphism increases. Metamorphic grade is a general term for describing the relative temperature and pressure conditions under which metamorphic rocks form.
metamorphism	The process of rock metamorphism changes the mineralogical and chemical composition, as well as the structure of rocks. Metamorphism is typically associated with elevated temperature and pressure; thus it

(continued on next page)

(continued)

Term	Definition
Metamorphic rock	affects rocks within the earth's crust and mantle. The process is driven by changing physical and/ or chemical conditions in response to large-scale geological dynamics.
Mineralization	Are rocks that developed their mineralogical and structural characteristics by metamorphic processes. From an engineering geological perspective, mineralization is the chemical alteration, replacement, and enrichment of minerals
Mineralogical characterization	Involves the study of minerals in terms of their size, habit, chemical composition, morphology, textural position, association and other attributes.
Paleozoic	It's a geological Era begins with the <a href="#">Cambrian Period</a> (541 million years ago) and ends with the <a href="#">Permian Period</a> (252 million years ago).
Petrographic characterization	Is the description and systematic classification of rocks, by examination of thin sections. Petrographic analysis would include determining properties such as grain size, texture, color, fractures, and abnormalities.
Precambrian	Is an informal term extensively used in the scientific literature to describe a large fraction of the <a href="#">Geological Time Scale</a> , extending from c. 4.560 to 541 million years ago. With boundaries respectively marking the origin of the Planet Earth and the appearance of <a href="#">fossils</a> suitable for systematic biostratigraphic correlation, this interval corresponds to almost 88 % of the Earth's existence.
Regional metamorphism	Occurs over wide areas, affects large volumes of rocks, and is associated with tectonic processes such as plate collision and <a href="#">crustal thickening</a> (orogenic metamorphism) and ocean-floor spreading (ocean-floor metamorphism). During the <a href="#">subsidence</a> of large basins, sedimentary piles can be
Retrograde metamorphism (diaphoresis, retrogressive metamorphism)	Is the mineralogical adjustment of relatively high-grade metamorphic rocks to temperatures lower than those of their initial metamorphism.
<a href="#">Rietveld refinement</a>	Is conducted by fitting a calculated <a href="#">diffraction pattern</a> to the observed data by adjusting each of the variables that describe the diffraction pattern.
Rock deformation	Is the result of tectonic events that are a unique function of time. With time, events such as <a href="#">magma</a> movement, faulting, earth quake, and fracturing occur in a cyclical form. It is recognized that the state of stress changes with time, affecting rock deformation directly.
Sedimentary rocks	Are formed from pre-existing rocks or pieces of once-living organisms. They form from deposits that accumulate on the Earth's surface. Sedimentary rocks often have distinctive layering or bedding.

## Declaration of generative AI and AI-assisted technologies in the writing process

**Statement:** During the preparation of this work, the author(s) used ChatGPT (OpenAI, San Francisco, California, USA, LLM). to improve language and readability of the paper. After using this tool, the author(s) reviewed and edited the content as needed and take (s) full responsibility for the content of the published article.

## Declaration of competing interest

The authors declare that they have no known competing financial interests or personal relationships that could have appeared to influence the work reported in this paper.

## Funding sources

This work was not supported by any external funding body or organization except the author's funding acquisition stated in Author contributions: CRediT, during the research stage.

## Acknowledgments

This study forms part of a Master of Science thesis project by the first author. The first author thanks the following individuals for their assistance with this study: Assoc.Prof. Dr. Mohamad Amran Mohd Salleh for the supervision of the master project. Dr. Muhammad Hatta Bin Roselee for the co-supervision, preparing the thin section, microscopic analysis, petrography, and the geology of the study area sections. Mr. Bushra Abdo Alsalam Omer Albashir for organizing field work and assistance with initial handspicemen identification. Mr. Ramah Othman for assisting in obtaining Sudanese Ministry of Minerals permission for transferring rocks from Sudan to Malaysia. Mr. Amjed Nassir Hamad for bringing the rock from Sudan to Malaysia by air. Ms. Aisyah.M.Yahya for assisting in EDS and XRD experiments. Elsevier Language Editing Services for the proofreading. Dr. Thavamaran Kanesan the Chief Editor of Proofreading by A UK PhD. Ms.Kelly Vellinga Chan for the proofreading. Ms.Dipika Roy Prapti for the proofreading. Assoc.Prof. Dr. Mohamad Amran Mohd Salleh, Dr.Muhammad Hatta Bin Roselee, and Dr.Suraya Abdul Rashid for their valuable review and editing. Thanks for the laboratory technicians of the mentioned laborites in 3 Materials and methods.

## Supplementary materials

Supplementary material associated with this article can be found, in the online version, at [doi:10.1016/j.sciaf.2025.e02602](https://doi.org/10.1016/j.sciaf.2025.e02602).

## References

- [1] C.J. Mitchell, Industrial Minerals Laboratory Manual: Flake Graphite, British Geological Survey, 1993. BGS Technical Report WG/92/30[Online]. Available: [https://nora.nerc.ac.uk/id/eprint/9015/1/Flake\\_graphite\\_lab\\_manual.pdf](https://nora.nerc.ac.uk/id/eprint/9015/1/Flake_graphite_lab_manual.pdf).
- [2] A.D. Jara, A. Betemariam, G. Woldetinsae, J.Y. Kim, Purification, application and current market trend of natural graphite: a review, *Int. J. Min. Sci. Technol.* 29 (5) (2019) 671–689, <https://doi.org/10.1016/j.ijmst.2019.04.003>.
- [3] D.D.L. Chung, Review: graphite, *J. Mater. Sci.* 37 (8) (2002) 1475–1489, <https://doi.org/10.1023/A:1014915307738>.
- [4] B.E. Lebrouhi, S. Baghi, B. Lamrani, E. Schall, T. Kouksou, Critical materials for electrical energy storage: li-ion batteries, *J. Energy Storage* 55 (2022) 105471, <https://doi.org/10.1016/j.est.2022.105471>.
- [5] J. Zhang, C. Liang, J.B. Dunn, Graphite flows in the U.S.: Insights into a key ingredient of energy transition, *Environ. Sci. Technol.* 57 (8) (2023) 3402–3414, <https://doi.org/10.1021/acs.est.2c08655>.
- [6] A. Ramji and K. Dayemo, "Releasing the pressure: understanding upstream graphite value chains and implications for supply diversification," 2024, doi: 10.7922/G2GQ6W38. [Online]. Available: <https://escholarship.org/uc/item/0q83t5fd>.
- [7] R. Klemm and D. Klemm, "Sequential and spatial distribution of gold mining sites in the Egyptian and Nubian Eastern Deserts," in *Gold and gold mining in ancient Egypt and Nubia: Geoarchaeology of the ancient gold mining sites in the Egyptian and Sudanese Eastern Deserts*, 2013, pp. 601–621, doi: 10.1007/978-3-642-22508-6\_7.
- [8] A.D. Jara, G. Woldetinsae, A. Betemariam, J.Y. Kim, Mineralogical and petrographic analysis on the flake graphite ore from Saba Boru area in Ethiopia, *Int. J. Min. Sci. Technol.* 30 (5) (2020) 715–721, <https://doi.org/10.1016/j.ijmst.2020.05.025>.
- [9] M.A.M. Mahmoud, A preliminary study of graphite-bearing rocks at Wadi Sikait area, South Eastern Desert, Egypt, *Arab. J. Geosci.* 6 (12) (2013) 4661–4669, <https://doi.org/10.1007/s12517-012-0712-5>. Dec.
- [10] C. Klein, A.R. Philpotts, *Earth Materials: Introduction to Mineralogy and Petrology*, 1st ed., Cambridge University Press, 2013.
- [11] A.A. Yassin, F.A. Khalil, A.G. El Shafie, Explanatory note to the geological map at the scale of 1:2,000,000 of the Democratic Republic of the Sudan, *Bull. Geol. Min. Res. Dept.* 35 (1984) 1–19.
- [12] R.J. Stern, A. Kröner, R. Bender, T. Reischmann, A.S. Dawoud, Precambrian basement around Wadi Halfa, Sudan: a new perspective on the evolution of the East Saharan Craton, *Geol. Rundsch.* 83 (3) (1994) 564–577, <https://doi.org/10.1007/BF00194162>.
- [13] M. Nafi, A. El Amein, M. El Dawi, K. Salih, O. Elbahi, A. Abou, Wadi Halfa oolitic ironstone Formation, Wadi Halfa and Argein areas, North Sudan, *Int. J. Environ. Ecol. Eng.* 9 (10) (2015) 1241–1246.
- [14] F.S. Reed, J.L. Mergner, Preparation of rock thin sections, *Am. Mineral.* 38 (1953) 1184–1203.
- [15] P.J. Laverge, Preparation of Geological materials for chemical and spectrographic analysis, Geological Survey of Canada, Department of Mines and Technical Surveys, Report 65-18, 1965. [Online]. Available: <https://emlibrary.gov.yk.ca/gsc/papers/65-18.pdf>.
- [16] W. Hildreth, J. Ryan-Davis, B. Harlow, Graphite in the Bishop Tuff and its effect on postcaldera oxygen fugacity, *Geosphere* 14 (1) (2018) 343–359, <https://doi.org/10.1130/GES01548.1>. Feb.
- [17] G.R.A. Kumara, et al., Development of a chemical-free floatation technology for the purification of vein graphite and characterization of the products, *Sci. Rep.* 11 (1) (2021) 22713, <https://doi.org/10.1038/s41598-021-02101-9>. Nov.
- [18] S. Febriana, E.S. Riyanto, A. Dimiyati, A. Handayani, Characterization studies of Cyclotron CS-30 carbon puller material using powder X-ray diffraction and SEM, EDX cross-section method, *IOP Conf. Ser. Mater. Sci. Eng.* 299 (2018) 012054, <https://doi.org/10.1088/1757-899X/299/1/012054>. Jan.
- [19] B. Shirley, E. Jarochowska, Chemical characterisation is rough: the impact of topography and measurement parameters on energy-dispersive X-ray spectroscopy in biominerals, *Facies* 68 (2) (2022) 7, <https://doi.org/10.1007/s10347-022-00645-4>. Apr.
- [20] V. Balaram, Current and emerging analytical techniques for geochemical and geochronological studies, *Geol. J.* 56 (5) (2021) 2300–2359, <https://doi.org/10.1002/gj.4005>. May.
- [21] M. Földvári, *Handbook of Thermogravimetric System of Minerals and Its Use in Geological Practice*, Geological Institute of Hungary, Budapest, Hungary, 2011.
- [22] A. Dharia, "Re: how does the type of gas atmosphere in TGA affect thermal residue (detailed and specific questions included)," ResearchGate. [Online]. Available: <https://www.researchgate.net/post/How-does-the-type-of-gas-atmosphere-in-TGA-affect-thermal-residue-detailed-and-specific-questions-included>.
- [23] W. Zhang, et al., A combined Raman spectroscopic and thermogravimetric analysis study on oxidation of coal with different ranks, *J. Anal. Methods Chem.* 2015 (2015) 1–8, <https://doi.org/10.1155/2015/306874>.
- [24] T.V. Petrova, R. Ferreira Mählmann, W.B. Stern, M. Frey, Application of combustion and DTA-TGA analysis to the study of metamorphic organic matter, *Swiss J. Geosci. Suppl.* 82 (1) (2002) 33–53. Jan.
- [25] M. Kirilova, et al., Structural disorder of graphite and implications for graphite thermometry, *Solid Earth* 9 (1) (2018) 223–231, <https://doi.org/10.5194/se-9-223-2018>. Feb.
- [26] J.H.T. Zethof, M. Leue, C. Vogel, S.W. Stoner, K. Kalbitz, Identifying and quantifying geogenic organic carbon in soils – the case of graphite, *Soil* 5 (2) (2019) 383–398, <https://doi.org/10.5194/soil-5-383-2019>. Dec.
- [27] J.M. Ferry, Petrology of graphitic sulfide-rich schists from south-central Maine: an example of desulfidation during prograde regional metamorphism, *Am. Mineral.* 66 (1981) 908–930.
- [28] I.S. Babiker, Z.K.A. Elsayed, A.H. El Nadi, Geological mapping and gold prospecting of Wadi Umm Beckol-Wadi Akasha area, northern Sudan based on remote sensing, *Int. J. Sci. Eng. Res.* 2 (6) (2015) 172–179.
- [29] J. Palosaari, R.M. Latonen, J.H. Smått, S. Raunio, O. Eklund, The flake graphite prospect of Piippumäki—An example of a high-quality graphite occurrence in a retrograde metamorphic terrain in Finland, *Miner. Depos.* 55 (4) (2020) 457–466, <https://doi.org/10.1007/s00126-020-00971-z>.
- [30] P. Sanyal, S.K. Bhattacharya, A. Sarkar, S. Acharyya, M.K. Bera, Origin of graphite, and temperature of metamorphism in Precambrian Eastern Ghats Mobile Belt, Orissa, India: a carbon isotope approach, *J. Asian Earth Sci.* 36 (4–5) (2009) 321–330, <https://doi.org/10.1016/j.jseas.2009.06.008>. Nov.
- [31] T. Al-Ani, S. Leinonen, T. Ahtola, D. Salvador, High-grade flake graphite deposits in metamorphic schist belt, central Finland—Mineralogy and beneficiation of graphite for lithium-ion battery applications, *Minerals* 10 (8) (2020) 680, <https://doi.org/10.3390/min10080680>.
- [32] D. Pascal, M. K. Ansdell, I.R. Annesley, T. Kotzer, Jiricka, "Graphite-bearing pelitic schists and their altered equivalents In the Dufferin Lake Zone, South-Central Athabasca Basin, Saskatchewan: constraints on Graphite formation and destruction, and implications for uranium mineralization, *Can. Mineral.* 54 (6) (2016) 1459–1491, <https://doi.org/10.3749/canmin.1600004>.
- [33] J.L. Urai, L.J. van Vliet, M. Krabbendam, Grain size stabilisation by dispersed graphite in a high-grade quartz mylonite: an example from Naxos (Greece), *J. Struct. Geol.* 25 (6) (2003) 855–866, [https://doi.org/10.1016/S0191-8141\(02\)00086-X](https://doi.org/10.1016/S0191-8141(02)00086-X).
- [34] T. Al-Ani, T. Ärvälä, K.C. Aarnio, A.T. Belozerovala, Metamorphic evolution of graphite in the paleoproterozoic Savo Schist Belt (SSB), Central Finland: constraints from geothermometric modeling, *Ore Geol. Rev.* 141 (2022), <https://doi.org/10.1016/j.oregeorev.2021.104672>.
- [35] J.X. Yui, E. Huang, Raman spectrum of carbonaceous material: a possible metamorphic grade indicator for low-grade metamorphic rocks, *J. Metamorph. Geol.* 14 (1) (1996) 115–124, <https://doi.org/10.1046/j.1525-1314.1996.05792.x>.
- [36] J. Jehlicka, O. Urban, J. Pokorný, Raman spectroscopy of carbon and solid bitumens in sedimentary and metamorphic rocks, *Spectrochim. Acta A Mol. Biomol. Spectrosc.* 59 (7) (2003) 1401–1408, [https://doi.org/10.1016/S1386-1425\(03\)00077-5](https://doi.org/10.1016/S1386-1425(03)00077-5).
- [37] W.A. Deer, R.A. Howie, J. Zussman, *An Introduction to the Rock-Forming Minerals*, Mineralogical Society of Great Britain and Ireland, London, U.K., 2013, <https://doi.org/10.1180/DHZ>.
- [38] C. Klein, *The 23rd edition of the manual of mineral science: (After James D. Dana)*, J. Wiley, Hoboken, NJ, 2008. Rev. ed. B. Dutrow, Ed.
- [39] M.E.P. Gomes, A.M.R. Neiva, Chemical zoning of muscovite from the Ervedosa granite, northern Portugal, *Mineral. Mag.* 64 (2) (2000) 347–358, <https://doi.org/10.1180/002646100549247>.
- [40] D. Craw, Geochemistry of late metamorphic hydrothermal alteration and graphitisation of host rock, Macraes gold mine, Otago Schist, New Zealand, *Chem. Geol.* 186 (1–2) (2002) 147–161, [https://doi.org/10.1016/S0009-2541\(02\)00139-0](https://doi.org/10.1016/S0009-2541(02)00139-0).

- [41] H. Terron, N.M. Ross, Mica polytypism: dissimilarities in the crystal structures of coexisting 1M and 2M biotite, *Am. Mineral.* 60 (1975) 1030–1040.
- [42] W.G. Mumme, G. Tsambourakis, I.C. Madsen, R.J. Hill, Improved petrological modal analyses from X-ray powder diffraction data by use of the Rietveld method; Part II, Selected sedimentary rocks, *J. Sediment. Res.* 66 (1) (1996) 132–138, <https://doi.org/10.1306/D42682D4-2B26-11D7-8648000102C1865D>.
- [43] C.A. Landis, Graphitization of dispersed carbonaceous material in metamorphic rocks, *Contrib. Mineral. Petrol.* 31 (4) (1971) 287–298, <https://doi.org/10.1007/bf00373366>.
- [44] E.S. Grew, Carbonaceous material in some metamorphic rocks of New England and other areas, *J. Geol.* 82 (5) (1974) 486–494, <https://doi.org/10.1086/627936>.
- [45] B. Wopenka, J.D. Pasteris, Structural characterization of kerogens to granulite-facies graphite: applicability of Raman microprobe spectroscopy, *Am. Mineral.* 78 (5–6) (1993) 533–538 [Online]. Available: <https://pubs.geoscienceworld.org/msa/ammin/article-abstract/78/5-6/533/42779/Structural-characterization-of-kerogens-to>.
- [46] H. Rantitsch, G. Lämmerer, W. Fisslthaler, E. Mitsche, S. Kaltenböck, On the discrimination of semi-graphite and graphite by Raman spectroscopy, *Int. J. Coal. Geol.* 165 (2016) 67–74, <https://doi.org/10.1016/j.coal.2016.04.001>.
- [47] B. Kwiecińska, H.I. Petersen, Graphite, semi-graphite, natural coke, and natural char classification—ICCP system, *Int. J. Coal. Geol.* 57 (2) (2004) 99–116, <https://doi.org/10.1016/j.coal.2003.09.003>.
- [48] B.K. Chakrabarti, “Chapter 6 - precambrian geotectonics in the Himalaya—Sans cenozoic hangover,” in *Precambrian Geotectonics in the Himalaya*, 2023, pp. 287–337. [10.1016/B978-0-323-91730-8.00006-7](https://doi.org/10.1016/B978-0-323-91730-8.00006-7).
- [49] T.V. Petrova, R.F. Mählmann, W.B. Stern, M. Frey, Application of combustion and DTA-TGA analysis to the study of metamorphic organic matter, *Schweiz. Mineral. Petrogr. Mitt.* 82 (2002) 33–53, <https://doi.org/10.5169/seals-62351>.
- [50] L. Xiaowei, R. Jean-Charles, Y. Suyuan, Effect of temperature on graphite oxidation behavior, *Nucl. Eng. Des.* 227 (3) (2004) 273–280, <https://doi.org/10.1016/j.nucengdes.2003.11.004>.
- [51] W.P. Barbara Kwiecińska, Thermal investigations of graphitic substances from metamorphic rocks, *Mineral. Pol.* 7 (2) (1976) [Online]. Available: <http://www.mineralogia.pl/PDFy/6%20-%20Vol.%207,%20No2,%201976.pdf>.
- [52] L.S. Majoros, K. Fintor, T. Koós, Metamorphic graphite from Szendrő (Szendrő Mts., NE-Hungary) detected by simultaneous DTA-TG, *J. Therm. Anal. Calorim.* 147 (2022) 3417–3425, <https://doi.org/10.1007/s10973-021-10713-6>.
- [53] A.M. Bishady, Mineralogy of graphite from the graphite-bearing schists of Wadi Lawi, South Eastern Desert, Egypt, *J. Geol. Resour. Eng.* 5 (4) (2017) 178–187, <https://doi.org/10.17265/2328-2193/2017.04.004>.
- [54] N. Vasumathi, et al., A mini review on flotation techniques and reagents used in graphite beneficiation, *Int. J. Chem. Eng.* 2023 (2023) 1–15, <https://doi.org/10.1155/2023/1007689>.
- [55] F. Syarifuddin, F.F. Florena, E.S. Hanam, N. Trisko, E. Kustiyanto, E. Enilisiana, A. Rianto, G. Arinton, Effect of acid leaching on upgrading the graphite concentrate from West Kalimantan (Indonesia), in: 1712, 2016 050022, <https://doi.org/10.1063/1.4941905>.